AGU PUBLICATIONS

JGR

Journal of Geophysical Research: Oceans

RESEARCH ARTICLE

10.1002/2014JC010506

Logarithmic velocity structure in the deep hypolimnetic waters of Lake Michigan

Cary Troy[1], David Cannon[1], Qian Liao[2], and Harvey Bootsma[3]

[1]Lyles School of Civil Engineering, Purdue University, West Lafayette, Indiana, USA, [2]Department of Civil and Environmental Engineering, University of Wisconsin-Milwaukee, Milwaukee, Wisconsin, USA, [3]School of Freshwater Science, University of Wisconsin-Milwaukee, Milwaukee, Wisconsin, USA

Key Points:
- Over 90% of near-bottom velocity profiles are logarithmic with median 1 m flow speed of 2.7 cm/s
- Fitted 1 m drag coefficient is 0.004 with hydrodynamic roughness of 0.12 cm
- The logarithmic layer thickness agrees with Ekman scaling and is found to be 0.07 u*/f

Correspondence to:
C. Troy,
troy@purdue.edu

Citation:
Troy, C., D. Cannon, Q. Liao, and H. Bootsma (2016), Logarithmic velocity structure in the deep hypolimnetic waters of Lake Michigan, *J. Geophys. Res. Oceans*, *121*, 949–965, doi:10.1002/2014JC010506.

Received 13 OCT 2014
Accepted 24 DEC 2015
Accepted article online 30 DEC 2015
Published online 27 JAN 2016

Abstract The characteristics of the bottom boundary layer are reported from a Lake Michigan field study carried out in deep hypolimnetic waters (55 m depth) during the stratified period (June–September 2012). The sandy substrate at the measurement site was densely covered with invasive quagga mussels (mean size: 1.6 cm; mean density: 10,000 mussels m^{-2}). The measurements reveal a sluggish, compact bottom boundary layer, with flow speeds at 1 mab less than 5 cm s^{-1} for most of the period, and a dominance of subinertial energy. A downwelling event caused the largest currents observed during the deployment (10 cm s^{-1} at 1 mab) and a logarithmic layer thickness of 15 m. In spite of the weak flow, logarithmic profile fitting carried out on high-resolution, near-bed velocity profiles show consistent logarithmic structure (90% of profiles). Flow was dominated by subinertial energy but strong modified by near-inertial waves. Fitted drag coefficients and roughness values are $C_{d1m} = 0.004$ and $z_0 = 0.12$ cm, respectively. These values increase with decreasing flow speed, but approach canonical values for 1 mab flow speeds exceeding 4 cm s^{-1}. The estimated vertical extent of the logarithmic region was compact, with a mean value of 1.2 m and temporal variation that is reasonably described by Ekman scaling, 0.07 u_*/f, and the estimated overall Ekman layer thickness was generally less than 10 m. Near-bed dissipation rates inferred from the law of the wall were $10^{-8}-10^{-7}$ W kg^{-1} and turbulent diffusivities were $10^{-4}-10^{-3}$ m^2s^{-1}.

1. Introduction

The characteristics of bottom boundary layers play an important role in determining the benthic exchange of nutrients, pollutants, and biota. This is especially true in the Laurentian Great Lakes, in the context of invasive dreissenids, whose effective filtration capacity of nutrients and biota is strongly linked to the hydrodynamics of the bottom boundary layer and the turbulent delivery of overlying water and its constituents [*Ackerman et al*., 2001; *Boegman et al*., 2008]. However, very few direct measurements exist of flow and turbulence in Great Lakes bottom boundary layers, especially in deeper waters – the focus of this paper - and these measurements are needed in order to support numerical modeling efforts of benthic exchange [e.g., *Luo et al*., 2012]. This paper provides results from direct near-bottom (<1 m above bottom, hereafter "mab") observations of boundary layer properties in the deeper waters of Lake Michigan.

Limited observations (including those presented here) suggest summertime deep water benthic energy levels in the Laurentian Great Lakes similar to those found in the deep ocean [e.g., *Sternberg*, 1970; *Wimbush and Munk*, 1970], with sluggish near-bottom currents generally less than 5 cm s^{-1} (at 1 mab) and presumably low associated turbulence levels. For Lake Michigan, this was found by *Saylor and Miller* [1988] (102 m depth), *Hawley and Lesht* [1995] (various depths >65 m) and more recently by *Choi et al*. [2012] for the center of Lake Michigan's southern basin (154 m depth). *Churchill et al*. [2004] report similar summertime benthic energy levels at 60 and 90 m depths in Lake Superior. In the context of mussel filtration, the weak benthic currents in Lake Michigan suggest that at least in these deeper waters, the vertical zone of filtration by invasive mussels will be limited by turbulent delivery to the lake bed, following arguments by *Koseff et al*. [1993].

In addition to the magnitude of offshore near-bottom currents, the vertical structure of these benthic boundary layers is also very important, because it determines the height of the turbulent boundary layer over which turbulent diffusion is appreciable, and what bulk transfer laws are applicable to model the

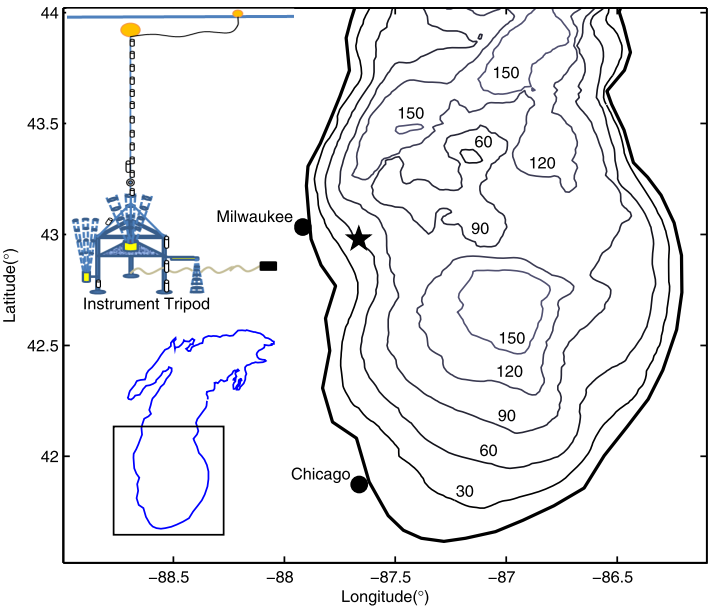

Figure 1. Field site location and instrument tripod schematic. The field site was located near Milwaukee, WI (USA). An instrumented tripod was placed along the lake bottom in 55 m-depth water, with three acoustic Doppler current profilers and a thermistor chain.

boundary transfer of mass and momentum. The theoretical starting point for the vertical structure of benthic boundary layers is typically the logarithmic velocity law (hereafter "log law"), which states that the mean (time-averaged) velocity $\bar{u}$ at an elevation z above the lake bed varies as

$$\frac{\bar{u}}{u_*} = \frac{1}{\kappa} \ln\left(\frac{z}{z_0}\right). \qquad (1)$$

Here u_* is the friction velocity ($u_* \equiv \sqrt{\tau_0/\rho}$, with τ_0 as the bottom stress and ρ the water density), κ is von Karman's constant (taken usually as 0.4), and z_0 is the roughness parameter particular to the substrate. The classic log law (1) is an extremely attractive formulation, because of the numerous theoretical results that can follow. One can use (1) to define a drag coefficient that allows for the conversion of a modeled or measured velocity, obtained at a reference elevation, to the bottom stress. Further, if a turbulent stress distribution is known or assumed, the vertical distribution of the vertical turbulent diffusivity can also be inferred via the Reynolds analogy. Hydrodynamic models of Lake Michigan have used various values of roughness to model bottom stress; these include $z_0 = 1$ cm [*Beletsky and Schwab*, 2001]; 0.1 cm [*Beletsky et al*., 2003]; 0.8 cm [*Lee et al*., 2007]; and 0.2 cm [*Anderson and Schwab*, 2013; *Bai et al*., 2013].

For rough, turbulent boundary layers, the log law (1) is expected to hold very close to the boundary, which in lakes has been found within the bottom 1 m of the water column [*Lorke et al*., 2002], i.e., within the blanking zone of most standard acoustic Doppler current profilers (ADCP). Very few measurements have been reported from within 1 mab in the Laurentian Great Lakes. In Lake Michigan, *Saylor and Miller* [1988] examined near-bed logarithmic structure during the stratified period at 100 m depth and found that velocity profiles between 1 and 9 mab were logarithmic only 19% of the time. Furthermore, fitted values of the 1 m drag coefficient and roughness were seen to approach canonical values ($z_0 \sim 10^{-1}$ cm) only when velocities at 1 mab exceeded 10 cm s^{-1}, which occurred less than 1% of the time (5 velocity profiles). Similar findings were reported by *Ackerman et al*. [2001] in shallower waters in Lake Erie, who saw logarithmic behavior less than 2% of the time and fitted roughness values exceeding 10 cm. In Lake Superior, *Churchill et al*. [2004] found limited logarithmic structure at deeper sites (60, 90 m depth), although their analysis was self-restricted to profiles where near-bed (1.3 mab) velocities exceeded 15 cm s^{-1}; all of the above work suggests that logarithmic structure is restricted to periods of elevated energy, which are rare in deeper waters, especially during the stratified period when baroclinic structure dominates [*Choi et al*., 2015]. However, recent work by *Valipour et al*. [2015a] showed consistent logarithmic structure in the bottom boundary layer ($<$ 1.5 mab) of Lake Erie's shallow central basin, with overlying stratification limiting the bottom mixed layer thickness.

When flow speeds are low, numerous effects can become appreciable, diminishing the height of the logarithmic layer and/or altering its form from (1). The most often investigated effects in oceanic and lake boundary layers include unsteadiness [*Friedrichs and Wright*, 1997; *Lorke et al*., 2002] and density stratification [*Grant and Madsen*, 1986; *Friedrichs and Wright*, 1997; *Perlin et al*., 2005; *Taylor and Sarkar*, 2008], both of which constrain the true logarithmic region to be close to the bottom. For a lake bottom boundary layer driven by an internal seiche, *Lorke et al*. [2002] found that the logarithmic layer height was strongly restricted by unsteadiness (generally to less than 0.5 mab), and that log law fits carried out above this

Table 1. Instrumentation Used in 2012 Lake Michigan Field Experiment[a]

Instrument	Depths Sampled	Sampling Scheme
Sontek 250 kHz ADCP	6.1:2.0:48.1 mab	10 min averagesevery hour
Sontek 3 MHz ADP	0.85:0.30:3.55 mab	10 min averagesevery hour
Nortek Aquadopp 2 MHz HR profiler	0.19:0.02:0.91 mab	8.5 min, 2 Hz (1024) burst every 3 h
HOBO proV2 Temperature loggers	0.25, 2.6, 5.0, 9.0, 13.0, 17.0, 21.0, 25.0, 29.0, 33.0, 37.0, 41.0, 45.0, 49.0 mab	Single meas. every 5 min
CTD	All	DOY 171,173,212,214,214,216,269

[a]Three velocimeters were mounted to the bottom tripod. Moored instruments were deployed from DOY 173–262.

region yielded erroneously high roughness and friction velocity values. At low speeds, viscosity can also become important, necessitating a smooth or transitional form of the log law [*Bowden*, 1978; *Ligrani and Moffat*, 1986]. And finally, in the context of invasive dreissenids (mussels) in the Great Lakes, mussel filtration may alter the vertical structure of near-bed flows when flow speeds are weak [e.g., *Monismith et al*., 1990; *Peine et al*., 2005; *van Duren et al*., 2006].

In this work we discuss observed properties of the bottom boundary layer at a deep water (55 m depth) site in Lake Michigan near Milwaukee, WI (USA), during the stratified period. The data set we describe involves more than 700 velocity profiles over a three month period. We employ a high-resolution velocity profiler to resolve the bottom 0.19–0.91 m of flow, in order to characterize the magnitude and drivers of near-bottom currents and stresses in Lake Michigan, and to resolve the true near-bed logarithmic layer. We assess the validity of the logarithmic law, and provide estimates of bottom stress and roughness that are generally unbiased by the confounding effects described above (e.g., stratification) because the logarithmic fitting is carried out on the true near-bed logarithmic layer. The paper is organized as follows: section 2 provides the details of the field observations; section 3 provides the observations, including fitted roughness/drag coefficient values and estimated boundary layer scales; and section 4 discusses the results in light of other relevant work and related issues.

2. Field Observations

Field observations were carried out for 3 months in Lake Michigan (near Milwaukee, WI, USA), in order to characterize the bottom boundary layer properties at a deep-water (55 m depth) location (Figure 1 and Table 1). The purpose of the measurements was to support the improvement of benthic exchange models in Lake Michigan. The measurements were taken between 21 June and 18 September in 2012 (DOY 173–262), during which we deployed a 2 m tall instrument tripod and an attached thermistor chain at the study site for the duration of the study (Figure 1).

Underwater imagery obtained near the mooring showed that the substrate at this location alternated between large expanses of pure sand and dense colonies of quagga mussels, and benthic sampling carried out at the mooring suggested strongly that the tripod was atop a dense mussel colony as shown in Figure 2. Mussel density and size class distribution were determined by multiple deployments of a ponar grab (20.5 cm × 20.5 cm sample area). Mean mussel density was 9968 m^{-2} (std. dev. = 3232 m^{-2}), with the majority of mussels (85%) being between 6 and 19 mm (mean length = 16.4 mm). Clearance rates measured for midsize mussels (13–17 mm) on two dates ranged from 2.2 to 4.4 L $mussel^{-1}$ d^{-1} [*Mosley and Bootsma*, 2015]. Following ASTM standard D422 [*ASTM*, 1998], a conventional sieve test was performed on a 300 g sample of dried bottom sediment collected with a ponar near the instrument tripod (11 sieves,

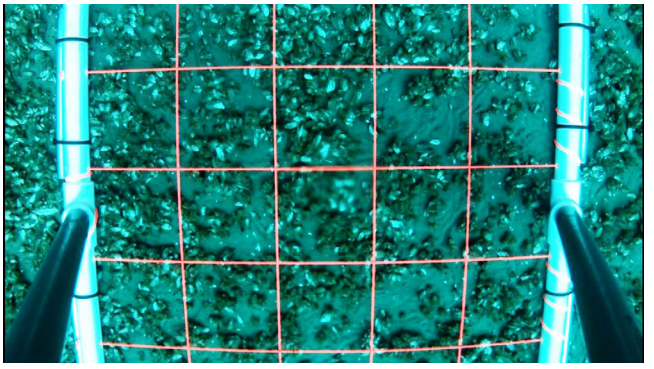

Figure 2. Underwater image of mussel-covered sandy substrate at measurement location near Milwaukee, WI. Each grid square is 10 cm × 10 cm.

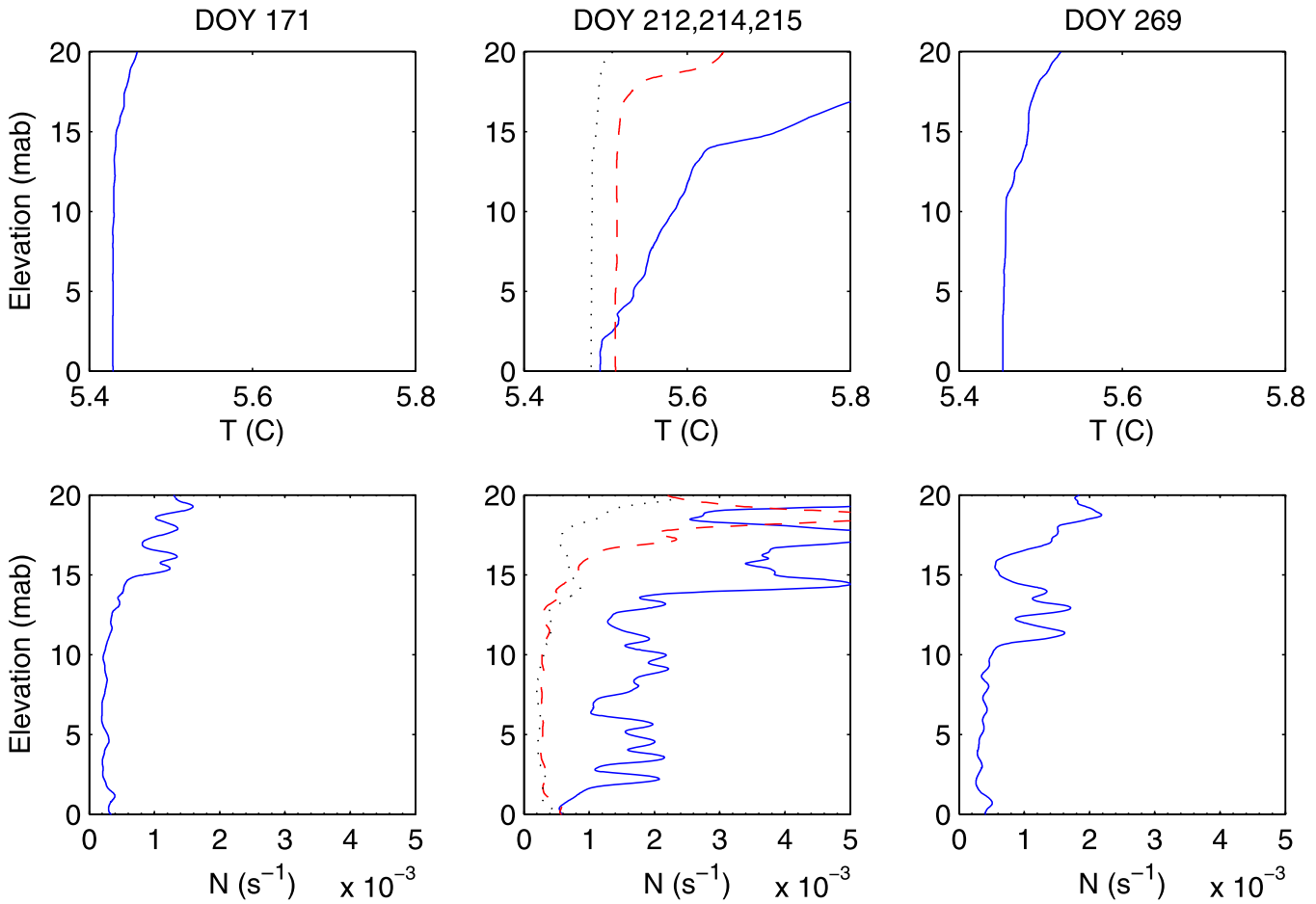

Figure 3. Observed near-bottom thermal stratification. Shown are data from 3 CTD sampling periods: (left) DOY 171; (middle) DOY 212, 214, 215 (gray, red, and blue respectively); and (right) DOY 269.

ranging from #4 to #400). The median sand diameter (d_{50}) determined from the analysis was 0.2 mm, with 15% of the sample by weight corresponding to fine sediments and clays (diameters less than 0.063 mm).

Water velocities were measured over nearly the entire water column using three acoustic velocimeters mounted to the 2 m tall bottom tripod (Figure 1 and Table 1): (1) an upward-looking, 250 kHz Sontek Acoustic Doppler Profiler (ADP) which recorded ten minute averages every hour, from 6.1–48.1 mab in 2 m bins; (2) an upward-looking, 3 MHz Sontek ADP which recorded ten minute averages every hour, from 0.85 to 3.55 mab in 0.30 m bins; and (3) a high-resolution 2 MHz Nortek Aquadopp HR profiler, downward looking, which provided high quality data between 0.19 mab and 0.91 mab, in 0.02 m bins. The HR profiler was burst sampled every 3 h, with 8.5 minute bursts of 2 Hz data. Estimated instrument uncertainties in the measured mean (burst-averaged) velocities are 11, 2.4, and 0.16 mm/s for the 250 kHz, 3 MHz, and 2 MHz profilers, respectively. The bottom boundary layer properties derived from logarithmic fit parameters provided herein are almost entirely obtained from the Nortek high-resolution profiler that resolved the 0.19–0.91 mab near-bottom region (see description of logarithmic fitting procedure in section 3.2).

The near-bottom overlapping region between the HR profiler data and the upward-looking 3 MHz ADP showed good agreement between the two instruments (R^2 =0.88, 0.94 between the two instruments' east, north currents at 0.85 mab, respectively), but in general the data from the two upward-looking ADP's were noisy relative to the HR profiler and not well-suited to the weak currents observed during the observations (28% more high-frequency energy in the ADP signal at 0.85 mab). Velocity data from between 10 mab and 15 mab were not usable for much of the deployment due to interference with the mooring line above the tripod, and are omitted from the analysis.

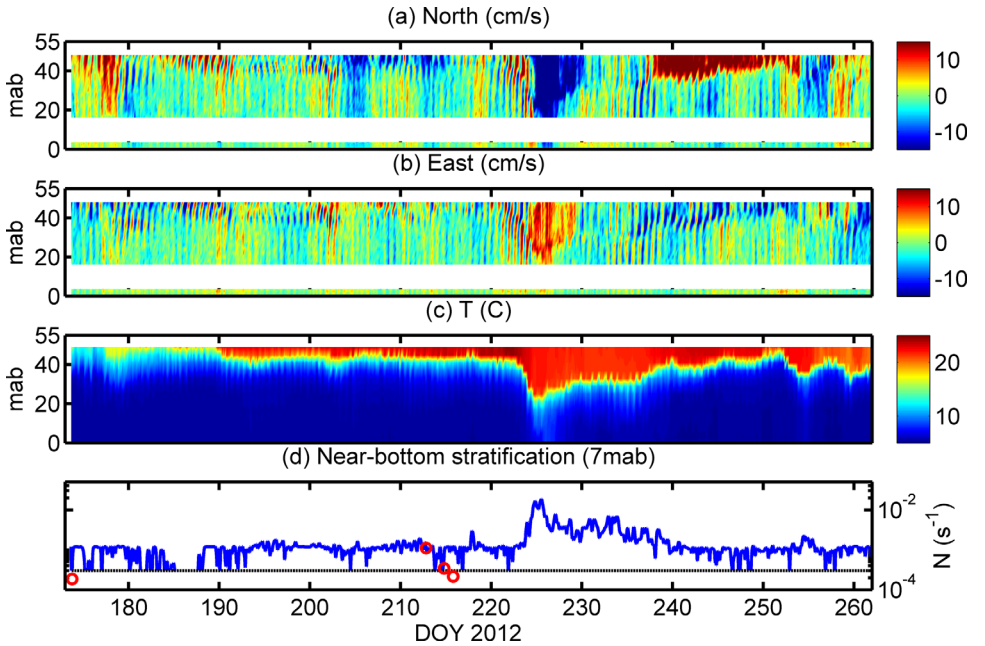

Figure 4. Measured velocities and temperatures for the experiment. Shown are (a) northward velocities and (b) eastward velocities. Whole water column temperatures are shown in Figure 4c, with mooring-estimated stratification at 7 mab shown in Figure 4d (solid blue line), CTD-derived values also at 7 mab (red circles), and the mininum stratification detection limit for the 7 mab estimate (dashed line). The large downwelling event is seen during DOY 223–230 as a (c) downwelled thermocline, (d) enhanced near-bottom stratification, and (a, b) strong currents.

Water column temperatures were measured with a vertical thermistor chain attached to the tripod. The thermistors were sampled every five minutes. In total 14 thermistors were deployed, measuring from 0.25 mab to 49 mab, with an average spacing of 4 m. CTD casts were also taken during the deployment, and used to corroborate the temperature chain measurements as well as to provide higher-resolution ($<$1 cm)vertical profiles (Table 1 and Figure 3). A continuous estimation of the Brunt-Väisälä frequency (N) was obtained at 7 mab by differentiating the temperature signals from sensors at 5 and 9 mab; careful comparison with CTD profiles indicated that this estimate was the closest-to-bottom accurate stratification measurement, with an estimated minimum detection level of 3 x 10^{-4} rad s^{-1}.

3. Results

3.1. Flow and Stratification

The water column was stratified for the entire deployment period, evolving from weak near-surface stratification (average $N = 0.03$ rad s^{-1} over the top 25 m, where N is the Brunt-Väisälä frequency) to a strong, deepening thermocline at the end of the deployment (Figure 4; $N = 0.1$ rad s^{-1} between 25 and 30 m depth). The base of the thermocline remained at least 20 m above the lake bottom at this location for the entire observation period except during a prolonged downwelling event (DOY 223–230). Bottom waters at the site were persistently between 5.3–5.6 C with the exception of the downwelling event, which raised near-bottom temperatures (2.5 mab) from 5.6 C (DOY 223.5) to a maximum of 8.5 C (DOY 226.1; Figure 4).

Near-bottom waters at 7 mab were weakly stratified for most of the observations (Figures 3 and4). Near-bottom stratification at this elevation was consistently at levels of $N \sim 10^{-3}$ rad s^{-1}, i.e., $N/f \sim 10$, where f is the Coriolis parameter ($f = 0.99 \times 10^{-4}$ rad s^{-1}, with a local inertial period of 17.6 h). Median N values obtained from finite differentiation between sensors were N= 0.0011, and 0.0012 rad s^{-1} for elevations of 7, and 11 mab, respectively. During the downwelling event (DOY 223–230), the N values were elevated to 0.0034, and 0.0061 rad s^{-1} for the same elevations, respectively (median values over this period), with brief maxima of 0.017 and 0.014 rad s^{-1} on DOY 225, the peak of the event.

In general the observed near-bottom velocities were weak, with velocities at 1 mab exceeding 5 cm s^{-1} only 7% of the time, a median current speed of 2.7 cm s^{-1}, and a range 0.1–10.4 cm s^{-1} (Figure 5). The strongest

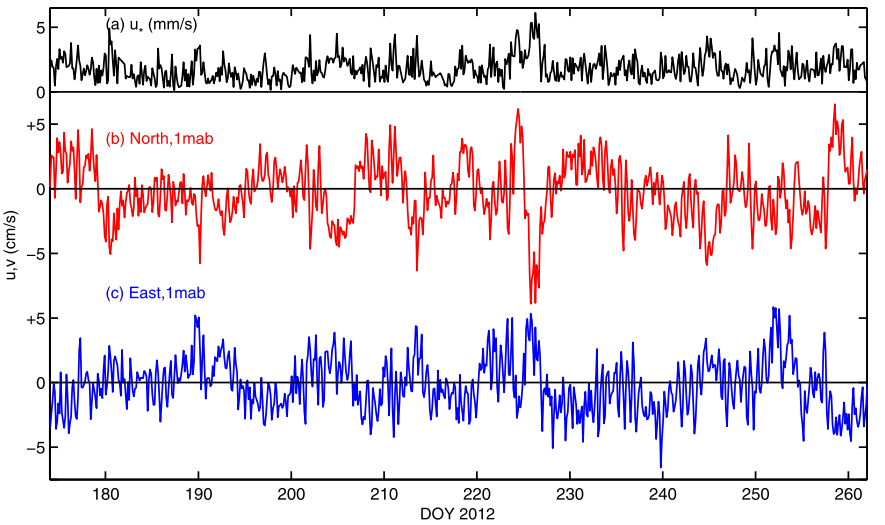

Figure 5. Log fit-derived friction velocity (a) and 1 mab velocities in the (b) north, and (c) east directions.

near-bottom flow during the deployment period was observed during the initial phase of the downwelling event, when 1 mab speeds briefly reached 10 cm s^{-1} (DOY 225.8). Surface flow was better aligned with the local coastline than near-bottom flow for most of the observations, with substantial cross-shelf near-bottom flow for much of the period, particularly from mid-July through early September (Figure 6).

The downwelling event (DOY 223–230) was initiated by a strong northerly wind event (estimated wind stress = 0.093 Pa) and characterized by a suddenly deepened thermocline and strong southward surface currents (37 cm s^{-1} at 9 m depth), which agrees with a simple geostrophic balance between an offshore barotropic pressure gradient and rotation, as *Troy et al.* [2012] found for upwelling along the Indiana coast

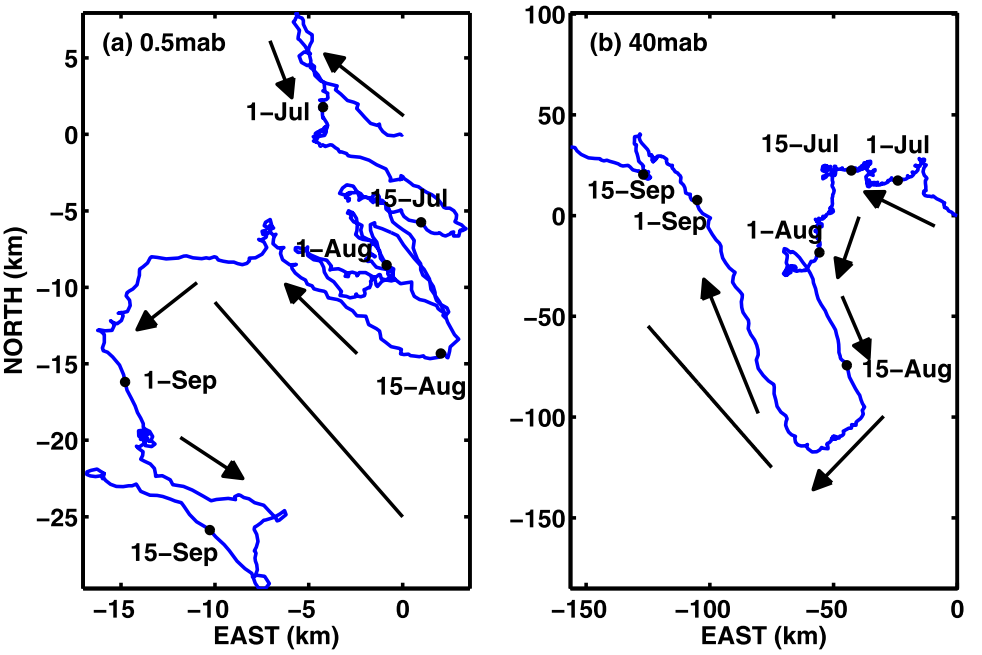

Figure 6. Particle pathlines (progressive vector diagrams) for (a) 0.5 and (b) 40 mab current measurements. Pathlines calculated by integrating observed velocities in time, starting at East and North positions of (0,0), with solid circles representing days as indicated. Also shown is the local isobath orientation as solid line; note that Figures 6a and 6b are scaled differently, as bottom currents are significantly weaker than surface currents.

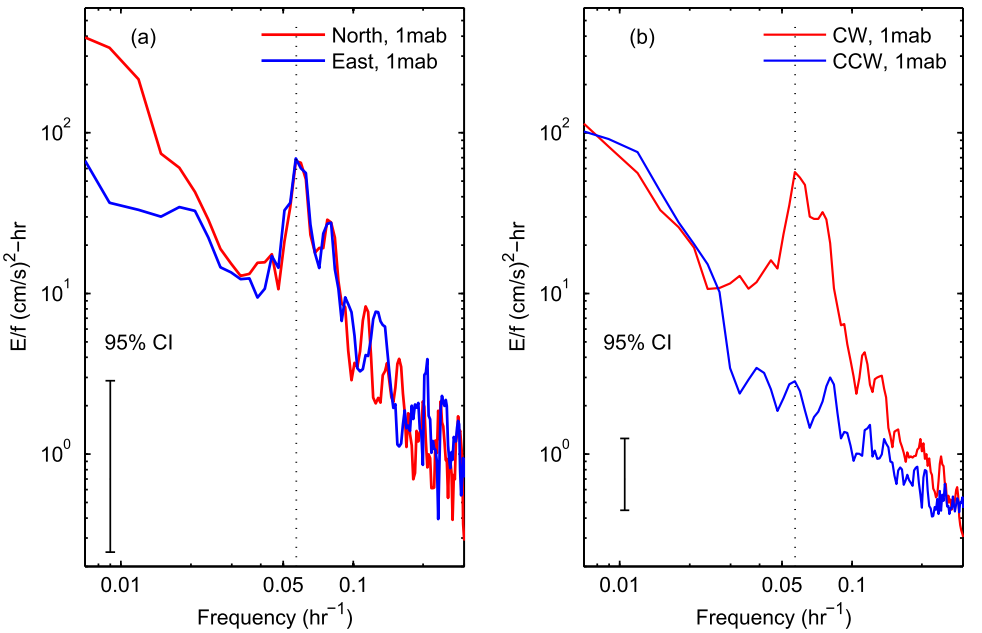

Figure 7. Power spectral densities of velocities at elevation of 1 mab. Spectra are calculated with two week windows and 4 point post-smoothing. Shown are (a) linear and (b) rotary spectra of the detrended north and east velocities at an elevation of 1 mab, with vertical lines in each plot denoting the local inertial period (17.6 h). The clockwise-rotating near-inertial energy is indicative of near-inertial internal Poincare waves [see *Choi et al.*, 2012].

of Lake Michigan. Satellite-derived lake surface temperatures derived from GLSEA (Great Lakes Surface Environmental Analysis, http://coastwatch.glerl.noaa.gov/) indicated that this event was associated with a broader downwelling region that occupied much of the Wisconsin coast. The downwelling slowly relaxed over a period of 3 weeks, eventually returning the thermocline to 12 m depth, before the thermocline began a steady deepening for the final period of the deployment (Figure 4). This downwelling was not expected since the Wisconsin coast is typically characterized by persistent upwelling during the summer period [*Plattner et al.*, 2006].

Near-bottom velocity spectra showed that most near-bottom energy is associated with subinertial (>17.6 h) flow processes, suggesting that the overall structure of the bottom boundary layer is expected to take the form of a bottom Ekman layer. Near-inertial waves do provide noticeable variability, particularly in the cross-shelf (east-west) direction (Figures 5–7). The relative energies contained in subinertial (>20 h), near-inertial (14–20 h), and high-frequency (<14 h) spectral bands are 75.6%, 12.3%, and 11.9% respectively for the north velocities, and 53.2%, 22.1%, and 24.5% for the east velocities. Within the near-inertial band (14–20 h), 94.6% of the energy is associated with clockwise rotation (Figure 7), indicating that the near-inertial energy is associated with basin-scale internal Poincare waves [*Choi et al.*, 2012; *Ahmed et al.*, 2014]. Additionally, while the overall percentage of near-inertial energy is modest, most of the local (super-inertial) maxima in both north and east currents occur when near-inertial currents add constructively with the subinertial flow (see Figure 5).

3.2. Logarithmic Law Fitting

To examine the vertical structure of near-bottom velocity profiles, burst-averaged velocity profiles were obtained by combining the measured velocities from the three profilers (excluding the zone 10–15 mab as mentioned previously). The mean of each 8.5 minute record was utilized from the bottommost profiler. At an elevation of 0.5 mab, mean velocities calculated after 4 minutes were converged to within 5% of the full 8.5 minute averages; after 7 minutes, profiles were found to be converged to within 1% of the 8.5 minute averages (median statistics).

To test the validity of the log law for the near-bottom velocity profiles, the log profile equation (1) was fit to the mean velocity profiles, with the friction velocity and roughness values as the fit parameters.

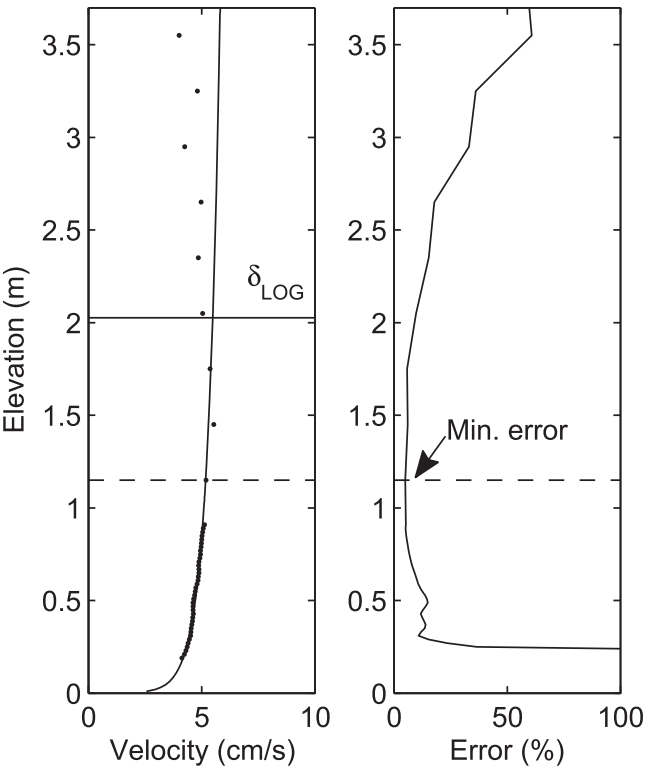

Figure 8. Sample fitted velocity profile and logarithmic fit. Shown are (a) fitted logarithmic profile atop measured data, with found logarithmic layer thickness δ_{LOG} as described in the text (~2 m for profile shown); and (b) the error in the fitted friction velocity as a function of profile length, showing the selection of the region for logarithmic profile fitting as the profile length that has the minimum error in the fitted friction velocity (data below the location of minimum error in the fitted friction velocity seen in Figure 8b, ~1.2 m for the profile shown).

The fitting procedure is straightforward but the selection of valid fits requires the adoption of a validity criterion for the fitted profiles (e.g., R^2 cutoff). Additionally, because the thickness of the logarithmic region is temporally variable (due to stratification, unsteadiness, etc.), it is desirable to have a fitting procedure that allows the fitting to be carried out over the near-bed region that is most logarithmic, i.e., the true logarithmic layer. This is for two reasons: (1) fits carried out with data outside the true logarithmic region will yield erroneous fit parameters; (2) it is desirable to use the entire logarithmic region in the fits in order to minimize the error in the fit parameters. The error in the fit parameters (u_*, z_0) is a function of both the R^2 value of the fit as well as the number of points in the profile [*Grant et al*., 1984; *Saylor and Miller*, 1988], and as such we adopted a fitting approach that minimizes the error in the fit parameters for each velocity profile, by selecting a fit region over which the error in the fit parameters is smallest, in lieu of an arbitrarily-imposed logarithmic region specification (e.g., bottom-most 0.5 m). The iterative procedure began by fitting a log profile to the three nearest-to-bottom points and was repeated on progressively longer profiles. The errors in the fitted parameters for each of the successively longer profiles were compared and the fitted profile having the smallest error in the fit parameters was selected as the best fit for that profile (Figure 8). Profiles yielding less than 15% error in the fitted friction velocity were selected as being acceptable (95% confidence interval). An alternate, nonoptimized fitting procedure, where the log law was simply fit to all data below 0.5 m, did not yield substantially different fit values than the optimization procedure above, and 97% of the optimized fits were for profiles less than 0.92 m. For all accepted fits, the estimated viscous sublayer thicknesses were less than 5 cm (the median theoretical sublayer thickness was 3 mm), validating that the fitting was indeed occurring in the logarithmic region and not in the viscous sublayer. Further details pertaining to the estimation of error in the fit parameters can be found in *Grant et al*. [1984] and *Saylor and Miller* [1988], and a sample fitted profile is shown in Figure 8.

The log law (1) fits the high-quality near bottom data quite well (Figures 9–11). Over the entire set of 715 profiles taken over 90 days, for which the median speed at 1 m elevation was 2.5 cm s^{-1}, we find the median R^2 value for all of the fits to be 0.984, with 674 profiles (94%) yielding fits with error less than 15% in the fitted friction velocity (for these good fits, the median R^2 is 0.990, with a median found profile length of 0.7 m and a median friction velocity error of 5%). As seen in Figure 9, the general trend with goodness of fit is that profiles with higher near-bottom speeds are more logarithmic, with the highest R^2 values corresponding to the swiftest flows ($R^2 > 0.9$ for $u_{1m} > 3$ cm s^{-1}). Our results suggest that the log law does consistently hold, within the bottom 1 m of the water column, even for the low-speed conditions seen during the measurements (median speed 2.5 cm s^{-1} at 1 mab).

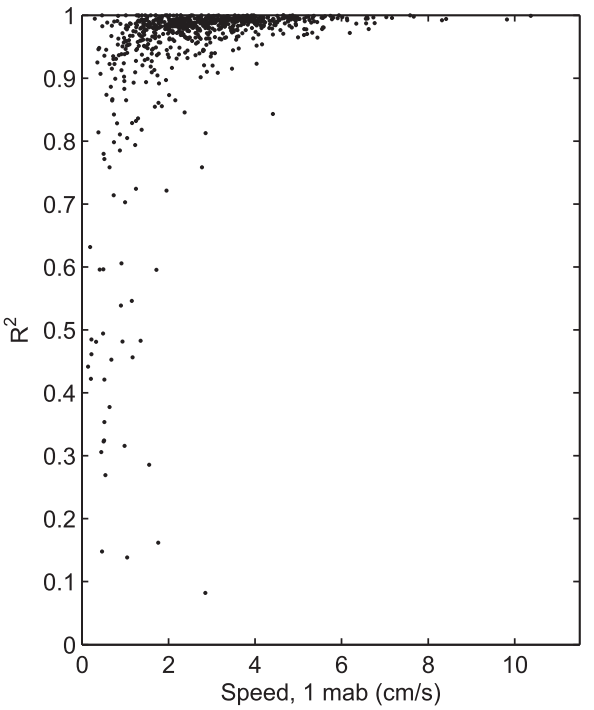

Figure 9. Goodness of fit for log law. Goodness of fit (R^2) for logarithmic fitting of near-bottom high-resolution velocity profiles. The general trend seen is that low speed flows have lower R^2 values for logarithmic fits, and vice-versa. The median R^2 value for all 715 profiles is 0.98.

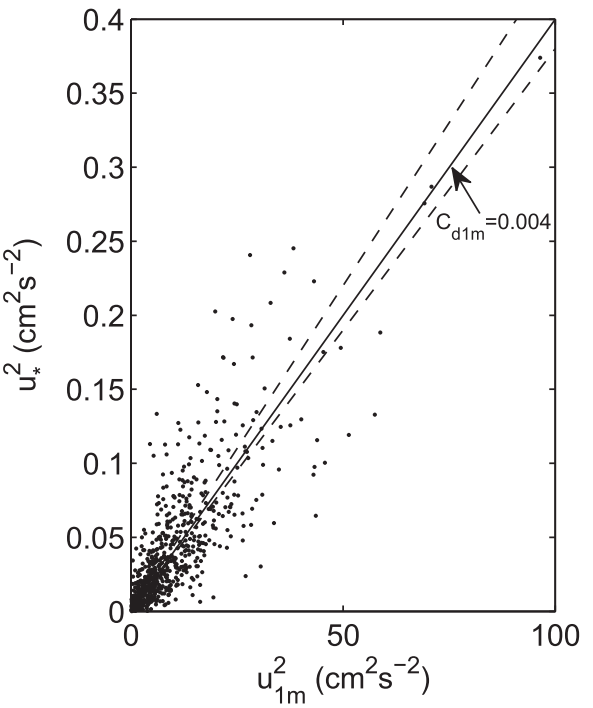

Figure 10. Fitted friction velocities versus 1 mab flow speed for logarithmic fitting. Shown are data (674 samples) for which the error in the fitted friction velocity is 15% or less. Also shown are lines denoting the median 1 mab drag coefficient (0.0040), and the associated bootstrapped 95% confidence interval values (C_{d1m} = 0.0038, 0.0044 for the lower, upper dashed lines, respectively).

In an attempt to quantify the height to which the logarithmic profiles actually held, vertical profiles of error between the fitted logarithmic profiles and observed data were examined. Above the high-resolution near-bottom data, the error generally appeared random, and inspection of these error profiles suggested that this mismatch (error) grew exponentially with distance from the bottom. As such, we fitted exponential functions to these vertical profiles of error, and from these fitted functions, determined the elevation at which the error was 10% of the fitted logarithmic profile value, deeming this the elevation to which the log law held (δ_{log}). This procedure revealed a median value for the logarithmic layer thickness of δ_{log} = 1.2 m and an instantaneous maximum of 14.7 m during the downwelling event, with 12 other instances during the event where the thickness exceeded 3 m. The found thickness of the logarithmic layer is discussed further in section 3.5.

3.3. Friction Velocities and Drag Coefficients

Statistics of the log law fit parameters are shown in Figure 12 and provided in Table 2. The estimated friction velocities span the range of u_* = 0.02–0.61 cm s^{-1}, with a median value of 0.17 cm s^{-1}. The observed friction velocities are well below the critical friction velocity for movement of the fine sand at the measurement location that is estimated with the Shields Diagram (1.5 cm s^{-1}).

The 1 m drag coefficient is defined here in the usual manner as

$$C_{d1m} = \frac{\tau_0}{\rho u_{1m}^2} = \frac{u_*^2}{u_{1m}^2}, \qquad (2)$$

where u_{1m} is the measured flow speed at 1 mab, and $\tau_0 = \rho u_*^2$ is the bed shear stress found from the log law fitting (Figure 10). Estimated 1 m drag coefficients are shown as a histogram in Figure 12 and as a bin-averaged function of 1 m flow speed in Figure 13. The measured drag coefficient exhibits higher variability at weak flow speeds, but generally when bin-averaged it is seen to be a weakly decreasing function of flow speed. The median 1 m drag coefficient over all profiles is 0.0040 (0.0038–0.0044 for bootstrapped 95% confidence interval, hereafter

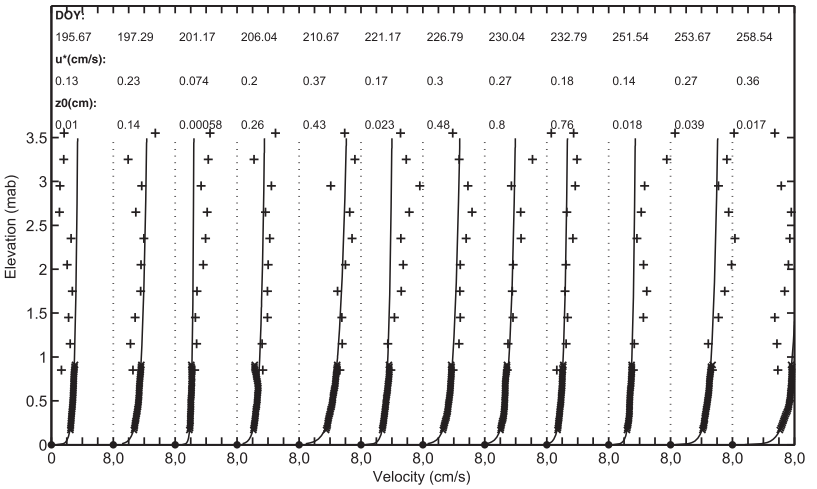

Figure 11. Randomly-selected velocity profiles and log-law fits over bottom 3.6 m for cases where the speed at 1 m elevation exceeds 2 cm/s and error in fitted friction velcity is 15% or less. Shown are velocity profile data over the bottom 3.6 m, which were obtained by the 2 MHz high-resolution profiler (<1 mab, "x") and the 3 MHz profiler (>0.85 mab, "+"). The solid line is the fitted log law, with the DOY, fitted friction velocities, and roughness values indicated above each profile.

"95% c.i."). For higher speeds ($u_{1m} > 5$ cm s^{-1}), the drag coefficient is slightly smaller, with a median value of 0.0035 (0.0029–0.0039, 95% c.i.).

The larger variation in the drag coefficient at low flow speeds (Figure 13; $\Delta C_{d1m} = 0.035$–3.5 for $u_{1m} <$ 1 cm/s, where ΔC_{d1m} is the 25th–75th percentile range) may be explained by the effects whose relative importance becomes larger with lower mean flow speeds, as discussed in the Introduction. The slightly larger *perceived magnitude* of drag coefficient at low flow speeds is consistent with the effects mentioned previously: near-bottom stratification, flow unsteadiness, and/or viscous effects. Additionally, elevated perceived drag coefficients and roughness values at low speeds can be seen in the presence of actively filtering mussels, whose excurrent jets can disrupt the structure of the boundary layer [*Monismith et al*., 1990; *Peine et al*., 2005, *van Duren et al*., 2006]. With regards to stratification, it is important to note that the actual effect of stratification – when important - is to *reduce* drag and roughness at low speeds, but the effect of stratification on fitted (perceived) values of drag and roughness is to create artificially *elevated* values at low speeds [*Friedrichs and Wright*, 1997]. However, limitations in our data––specifically the lack of stratification measurements within 1 mab and the near-bed velocity sampling rate (every hour for the 3 MHz ADP at 0.85 and upward; every 3 h for the 2 MHz HR Profiler sampling 0.91 mab and below)––preclude the quantification of these effects at low speeds.

3.4. Roughness

The median fitted roughness values for all flow speeds is $z_0 = 0.12$ cm (0.10–0.15 cm, 95% c.i.), and this value shows considerable scatter, but primarily for low flow speeds (Figures (10 and 12), and 13), with the roughness value decreasing slightly for higher speeds (median z_0=0.07 cm (0.04–0.10 cm, 95% c.i.), for $u_{1m} > 0.05$ cm s^{-1}). If one assumes that the log law holds to 1 m elevation, then the fitted roughness can be converted to a 1 m drag coefficient by rearranging the log law (1) as: $C_{d_{z_0}} = \left[\frac{1}{\kappa} log\left(\frac{z}{z_0}\right)\right]^{-2}$, where z = 1 m. The median roughness-inferred drag coefficient is $C_{d_{z_0}} = 0.0035$ (0.0033–0.0037, 95% c.i.), which is consistent with the actual measured drag coefficient (0.0040), suggesting that the log law does in the median hold to 1 m elevation, as was found with the exponential distribution error estimation technique described previously.

For fully-rough flow, the equivalent sand grain roughness (k_s) can be inferred from z_0 as $k_s = e^{8.5\kappa} z_0 = 32.6\, z_0$ for $\kappa = 0.41$ [*Van Rijn*, 1993; *Pope*, 2000; *Nielsen*, 2005]. If we assume that the boundary layer was hydrodynamically rough at the highest flow speeds ($u_{1m} > 5$ cm s^{-1}), for which the median roughness is z_0= 0.07 cm (Figure 13), the equivalent sand grain roughness is obtained as $k_s = 2.2$ cm (1.3–3.5 cm, 95% c.i.), a value 11 times larger than the true sand grain size at the site ($d_{50} = 0.2$ mm), which affirms that larger

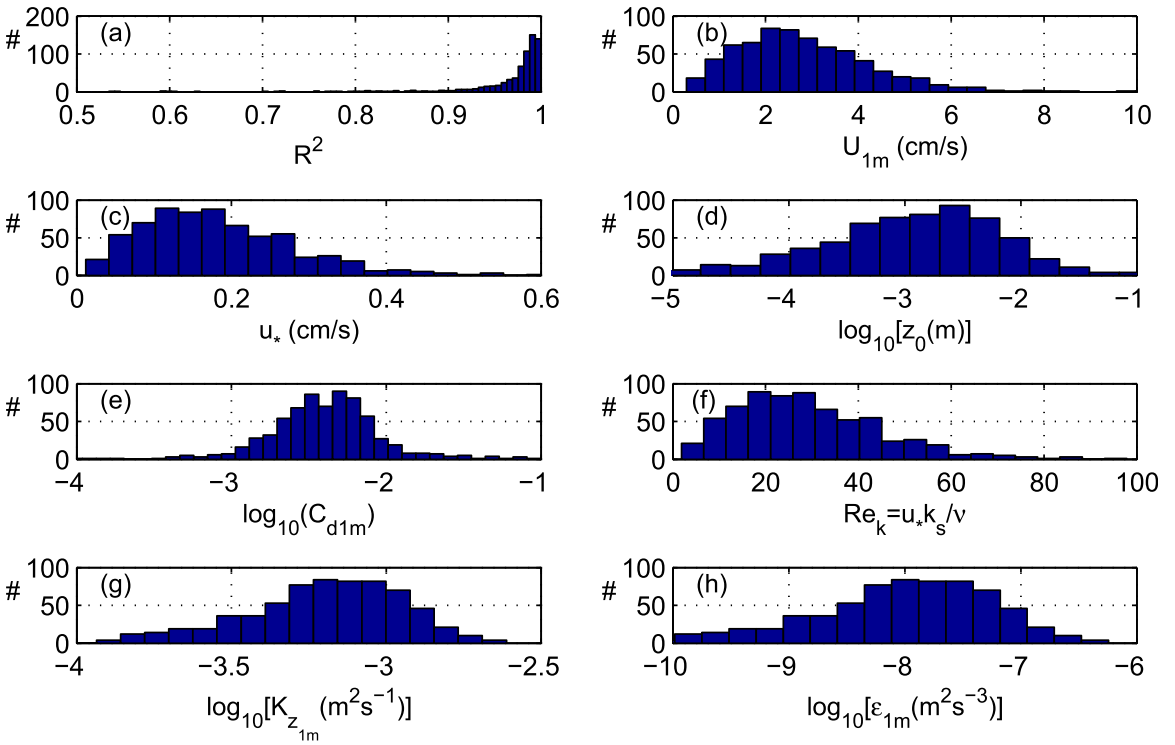

Figure 12. Histograms of measured bottom boundary layer and fitted log law parameters. Shown are histograms of (a) R2 values for all log law fits; (b) observed 1 mab flow speeds; (c) log law-derived friction velocities; (d) log law roughness parameter (z_0); (e) 1 mab drag coefficient; (f) estimated roughness Reynolds numbers; (g) law of the wall (LOW) estimate turbulent diffusion coefficient at 1 mab ($K_{z,LOW} = u_* \kappa z$, m^2 s^{-1}); law of the wall (LOW) estimate for turbulent dissipation at 1 mab ($\epsilon_{LOW} = \frac{u_*^3}{\kappa z}$, m^2 s^{-3}). 715 total samples were used for Figures 12a and 12b; 674 samples were used for Figures 12c–12h.

scale roughness elements – most likely the dense beds of quagga mussels - are likely the cause of the observed hydrodynamic roughness.

Because of the low speeds associated with the boundary layer, the possibility exists that the flow is not fully rough, and this appears to be the case for many of the observed profiles. Using the above median roughness value $k_s = 2.2$ cm, the roughness Reynolds numbers ($Re_k = u_* k_s \nu^{-1}$) associated with the measurements have a range $2.6 < Re_k < 133$ (Figure 12 and Table 2), which generally fall in the transitional region defined in laboratory studies ($2.25 < Re_k < 90$) [*Ligrani and Moffat*, 1986]. Similar findings were reported for oceanic and estuarine boundary layers in early work by *Sternburg* [1970] and *Wimbush and Munk* [1970].

3.5. Boundary Layer Length Scales

Because the boundary layer at the measurement location is dominated by subinertial energy, it is expected to have the characteristics of a bottom Ekman layer [see e.g., *Cushman-Roisin and Beckers*, 2011]. In the northern hemisphere, unstratified bottom Ekman layers in the ocean have currents that veer counter-clockwise as the boundary is approached, and observations generally show approximately 15° of veering over an overall Ekman layer thickness of $\delta_E \approx 0.4\, u_*/f$, and an oft-cited logarithmic layer thickness of approximately 10% of δ_E [*Grant and Madsen*, 1986; *Cushman-Roisin and Beckers*, 2011; *Perlin*

Table 2. Bottom Boundary Layer Parameters Inferred From Lake Michigan Field Observations and Logarithmic Profile Fitting[a]

Quantity (Units)	Median Value, ± One std. Deviation† or Bootstrapped 95% Confidence Interval††
Speed at 1 mab, U_{1m} (cm/s)	2.5, ± 1.5† (max: 10.4)
Friction velocity, u_* (cm/s)	0.17 ± 0.10† (max: 0.61)
Roughness, z_0 (cm)	0.12 (0.10–0.15) ††
Drag coefficient at 1 mab, C_{d1m}	0.0040 (0.0038–0.0044)††
LOW dissipation at 1 mab, $\log_{10}(\epsilon_{1m}$ (m^{2}s^{-3}))	−7.9 ± 0.8† (max: −6.2)
LOW turbulent diffusivity at 1 mab, $\log_{10}(K_{z1m}$(m^{2}s^{-1}))	−3.1 ± 0.3† (max: −2.6)
Roughness Reynolds number, Re_k	24 ± 14† (max: 90)

[a]The significance of the † and †† symbols in this table is defined in the column heading for the second column. In other words, the † denotes ± one std. deviation, and the †† denotes bootstrapped 95% confidence interval.

et al., 2007]. With the observed values of u_*, the corresponding estimated unstratified Ekman layer thicknesses span the range $\delta_E \frac{0.4u_*}{f}$ 3.2 – 17 m with a median value of 6.8 m (Figure 14; values are smoothed with a 36 h window). Our attempts to corroborate this estimate with calculations of veering angles, following *Perlin et al*. [2007], did not produce meaningful results due to noise in the upward-looking profilers' data above 1 mab and the lost data between 10 and 15 mab.

Near-bottom stratification can alter the structure and reduce the thickness of a bottom Ekman layer (and the near-bed logarithmic layer) [see e.g., *Perlin et al*., 2005; *Taylor and Sarkar*, 2008]. *Taylor and Sarkar* [2008] carried out numerical simulations of a stratified turbulent Ekman layer, with stratification imposed from above (as is most likely the present case for Lake Michigan late in the stratified period when sediments are in thermal equilibrium with overlying water), for a turbulent Reynolds number and stratification range very similar to our observations. Their simulated reduced Ekman thicknesses for near-bottom stratification levels of $\frac{N}{f} = 32$ and 75 are reasonably reproduced by *Pollard et al*.'s [1972] simple formula:

$$\delta_E = \frac{1.7}{\sqrt{N/f}} \left(\frac{u_*}{f}\right) \tag{3}$$

(this formula gives generally similar results to those of *Weatherly and Martin* [1978] and *Zilitinkevich et al*. [2002], the former of which showed good agreement with recent observations in Lake Erie by *Valipour et al*. [2015a]). Comparing this reduced thickness to the estimated unstratified Ekman thickness reduced according to the three formulae cited above indicate that the Ekman layer thickness was reduced during the period of relatively strong near-bottom stratification that was associated with the downwelling event (Figure 14).

The height of the found logarithmic layer (δ_{log}) found with the procedure described previously is shown in Figure 14; this thickness is very well-approximated for most of the period as $\delta_{LOG} = 0.07u_*/f$. The scaling constant of 0.07 is slightly larger than what has been found and cited for other low-frequency unstratified oceanic and atmospheric boundary layer studies and reviews (0.03: *Tennekes* [1973]; 0.04: *Grant and Madsen* [1986]; 0.04: *Lueck and Lu* [1997]), but lower than that reported by *Taylor and Sarkar* [2008, ~0.11, see their Figure 8] for numerical simulations of a turbulent Ekman layer.

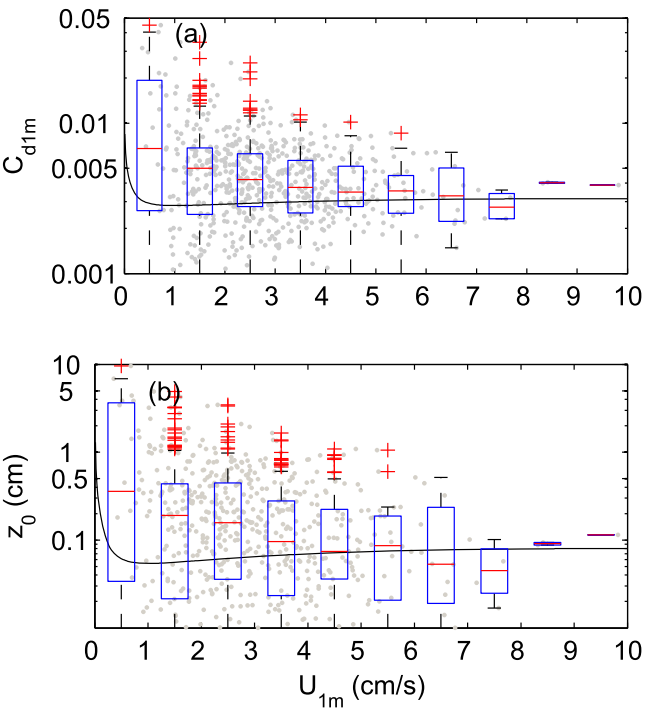

Figure 13. (a) Fitted 1m drag coefficient and (b) roughness values verses 1 m flow speed. Data are aggregated into 1 cm/s speed bins, with boxplots given for each speed bin to show variability within bins. Red lines indicate median values within boxes; the boxes span the 25th–75th percentiles of data within bins; points outside the whiskers are outliers, denoted as +. Also shown as solid lines are the theoretical dependences for drag coefficient and roughness as given by *Ligrani and Moffat* [1986], which account for boundary layer transition from smooth to rough as flow speed increases.

While various modified logarithmic profiles exist to account for near-bed stratification [e.g., *Friedrichs and Wright*, 1997; *Perlin et al*., 2005; *Taylor and Sarkar*, 2008], the lack of near-bed stratification measurements precluded their application to the present observations. Additionally, no dependence of the logarithmic layer thickness on the nearest-to-bottom stratification (7 mab) could be discerned from the data. However, as mentioned previously, the most strongly-stratified episode of the deployment—the downwelling event—was when the largest instantaneous logarithmic layer thicknesses were estimated. This seems counterintuitive at first, since stratification should reduce the logarithmic layer thicknesses, but the downwelling event created the strongest observed currents and friction velocities, and the net

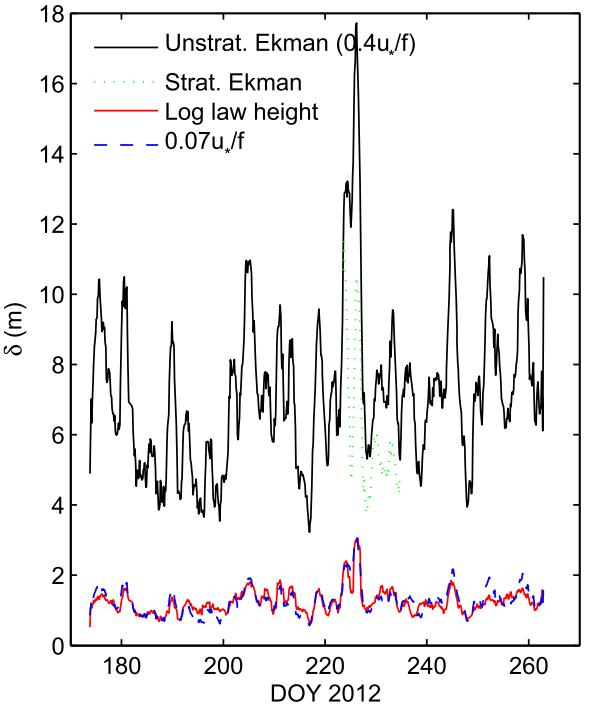

Figure 14. Boundary layer thicknesses. Shown are the unstratified Ekman layer thickness ($\delta_E = 0.4\ u_*/f$); the stratified Ekman layer thickness, when less than the unstratified thickness [*Pollard et al.*, 1972] ($\delta_E = 1.7\ u_*/\sqrt{Nf}$); the found height of the logarithmic layer (δ_{LOG}), as described in the text; and a line of $0.07\ u_*/f$. Layer thicknesses are smoothed with a 36 h moving average.

effect was still to increase the thickness of the logarithmic layer. Additionally, the Ekman layer thickness responds at a much slower (inertial) timescale than the logarithmic layer.

4. Discussion and Conclusions

The high-resolution velocity profiles taken here in the deeper hypolimnetic waters of Lake Michigan during the stratified period demonstrate conclusively that even in low-energy environments, velocity profiles very near to the boundary (<1 mab in the present case) can exhibit consistent logarithmic structure, which we suggest is a consequence of the subinertial dominance in the flow structure. Over 90% of the velocity profiles taken over the 90 day period yielded acceptable logarithmic fits, with median fit values of drag coefficient ($C_{d1m} = 0.004$) and roughness ($z_0 = 0.12$ cm) close to other values reported in oceanic and large lake environments. This includes the deep water and tidal channel ocean measurements by *Sternberg* [1968, 1970] (C_{d1m} =0.002–0.004); continental shelf measurements by *Grant et al.* [1984] ($C_{d1m} = 0.004$, when surface wave effects were absent), the Baltic Sea [*Van der Lee and Umlauf*, 2011] ($C_{d1m} \approx 0.002$), limited Lake Michigan measurements by *Saylor and Miller* [1988] ($C_{d1m} = 0.0031$–0.0066, for $u_{1m} > 10$ cm s^{-1}), Lake Superior [*Churchill et al.*, 2004] ($C_{d1m} = 0.002$–0.003, for 1.2 mab speeds exceeding 15 cm s^{-1}), and most recently Lake Erie's stratified central basin [*Valipour et al.*, 2015a] ($C_{d1m} = 0.0042$–0.0048).

The roughness and drag values reported here and for Lake Erie [*Valipour et al.*, 2015a] are lower than those reported by *Lorke et al.* [2002] for Lake Alpnach (C_{d1m}=0.009), which *Valipour et al.* [2015a] attribute to differences in substrate sediment roughness; the elevated Lake Alpnach values may also be due to the high degree of unsteadiness in their internal seiche-driven system, and the lack of measurements within the bottommost 0.5 m, both of which can contribute to deviations from the law of the wall [*Friedrichs and Wright*, 1997].

The logarithmic law proves so robust for the present observations and environment for a combination of reasons. Firstly, while stratification may have briefly limited the overall (Ekman) boundary layer thickness during the observed downwelling event, the very near-bed zone over which the velocity measurements occurred was unaffected by stratification, precluding stratification-related modifications to the log law for this region [*Friedrichs and Wright*, 1997; *Perlin et al.*, 2005, 2007; *Taylor and Sarkar*, 2008]. That is not to say that stratification would not provide important modifications to the flow outside of this very near-bed region.

Secondly, the flow at the measurement site was dominated by near-inertial and subinertial processes, and thus any near-bed modification to the log law due to unsteadiness should be absent. This is in contrast to bottom boundary layers in smaller lakes driven by high-frequency internal seiches for which the unsteadiness in the driving flow serves to strongly modify even very near-bed velocity structure [e.g., *Lorke et al.*, 2002; *Lorke*, 2007]. The sub and near-inertial dominance in the deep Lake Michigan waters examined here are also different than Lake Erie's shallow central basin, which is affected by both near-inertial internal Poincaré waves [*Valipour et al.*, 2015b] as well as surface seiches [*Bouffard et al.*, 2012]. Additionally, while the "deep" site examined here (55 m deep) is not deep by oceanic standards, Lake Michigan's limited fetch and summer wind characteristics (weak and southwesterly [*Troy et al.*, 2012]) generally do not create summer surface waves at the field site that affect the bottom boundary layer (however, this is not true for

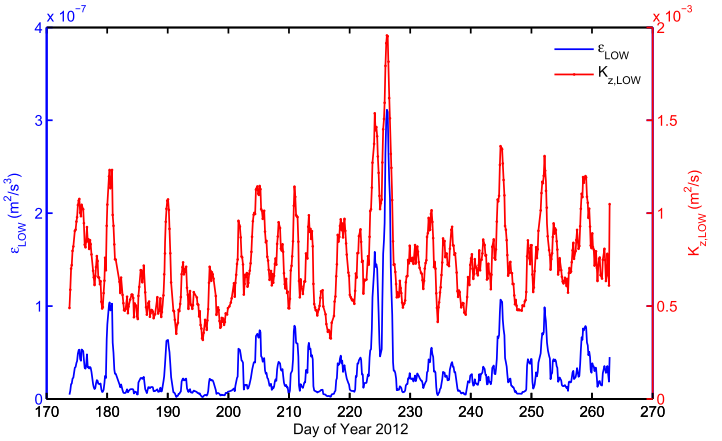

Figure 15. Law-of-the-wall estimates for turbulent dissipation ($u_*^3/\kappa z$) and turbulent diffusion coefficient ($u_*\kappa z$) at an elevation of 1 mab.

winter). Thus there is no expected modification to the near-bed log law due to surface waves as is often seen in coastal waters of comparable depth [e.g., *Grant et al.*, 1984; *Grant and Madsen*, 1986; *Mellor*, 2002].

Friction velocities at the site were in the range $u_* = 0.02$–0.61 cm s^{-1}, with a median value of 0.17 cm s^{-1}. Estimates of the roughness Reynolds number suggest that the boundary layer roughness classification was primarily transitional in nature (with regards to smooth versus rough), with only several high-speed episodes producing a fully rough boundary layer. However, the weakest flows observed did not yield roughness and drag values consistent with expected smooth or transitional boundary layer formulations [e.g., *Ligrani and Moffat*, 1986], suggesting that viscous effects were not responsible for the observed elevated roughness and drag values at low speeds. This is identical to what was reported by *Sternberg* [1968, 1970] and summarized in *Bowden* [1978], but to our knowledge, aside from the recent work by *Wengrove and Foster* [2014] and *Valipour et al.* [2015a], near-bed viscous effects on the log law and the viscous sublayer in oceanic and lake boundary layers have not received much attention since these early studies. *Valipour et al.* [2015a] classified the bottom boundary layer in Lake Erie's central basin as hydraulically smooth, but it is important to note that they used the actual sediment sand grain size for the roughness scale in their classification estimate ($\sim 10^{-5}$ m), and not their found roughness value ($k_s \sim 30\, z_0 \sim 0.06$ m) [see e.g., *van Rijn*, 1993]. Using found (fitted) roughness values (z_0) and the conversion $k_s = 32.6\, z_0$ [*van Rijn*, 1993], for mean reported values one obtains a transitional classification for the present Lake Michigan measurements and fully rough classifications for both Lake Erie [*Valipour et al.*, 2015a] (taking $\bar{u_*} = 0.25$ cm s^{-1}, $\bar{z_0} = 0.22$ cm, $\bar{T} = 10$ C) and Lake Alpnach [*Lorke et al.*, 2002] (taking $\bar{u_*} = 0.2$ cm s^{-1}, $\bar{z_0} = 1.4$ cm, $\bar{T} = 5$ C). In other words, the boundary layers for all three measurement sites would be classified as smooth with respect to the actual sediment roughness (assuming $u_* \sim 10^{-1}$ cm s^{-1} and sediment diameters 10^{-4} m and smaller, which is reasonable for all three systems, yielding $Re_k < O(1)$), but transitional/rough with respect to the effective roughness, which is presumably set by larger-scale sediment features. However, it is difficult to further this comparison without more detailed knowledge of site roughness characteristics – particularly macro-roughness – and/or measurements much closer to the substrates at these sites.

A simple estimate of the mean theoretical viscous sublayer thickness in the present case is $5\,\nu/u_* \sim 3$ mm [e.g., *Pope*, 2000], which places the viscous sublayer well below the bottommost measurement (in the mean), i.e., not discernable with our data as *Caldwell and Chriss* [1979] were able to detect. However, in quagga mussel-infested Lake Michigan (Figure 2), the concept of a viscous sublayer is somewhat dubious, at least over dense mussel beds, given the size of the mussels ($\sim$16 mm) and the effects of mussel filtration on the flow in contact with the lake bed, which would likely break up this layer. In spite of the near-bed resolution employed in the present study (0.19 mab for lowest measurement), closer-to-bottom measurements are needed to truly resolve the effects of mussels on the overlying flow.

Estimates of various boundary layer scales revealed that the thickness of the logarithmic layer was found to be approximately 17% of the theoretical unstratified Ekman layer thickness ($0.4u_*/f$), with a median value of 1.2 m, i.e., 0.07 u_*/f. This estimate may serve as a guide in other low-frequency, unstratified boundary layer studies and modeling efforts where log profile resolution or application is important.

Turbulent quantities inferred from the law-of-the-wall (LOW) at 1 mab for the present measurements compare well with published bottom boundary layer values for hypolimnetic waters in systems with similar energy and stratification levels. Our inferred kinetic energy dissipation rates ($<\epsilon_{1m}> = <u_*^3>/\kappa$ z = 1.3×10^{-8} $m^2 s^{-3}$) and vertical diffusivities at 1 mab ($<K_{z1m}> = <u_*>\kappa z = 7.9 \times 10^{-4}$ $m^2 s^{-1}$) are presented in Table 2 and Figure 15. These values are similar to measurements by *Van der Lee and Umlauf* [2011, Baltic

Sea, see their Figure 6], and slightly smaller than those reported by *Ravens et al*. [2000, Lake Baikal, see their Table 2 and Figure 5]; both the Baltic Sea and Lake Baikal observations are similar to the present field site as they have hypolimnetic currents dominated by near- and subinertial processes. Our inferred LOW turbulent diffusivities substantially higher than those reported in smaller lakes with stronger currents [e.g., *Lorke*, 2007; *Cossu and Wells*, 2013]; this is because of the near-bottom stratification present for those studies which, when parameterized, yields lower estimates for the turbulent diffusivity than the unstratified LOW estimate. The same arguments hold true for Lake Erie's central basin, which yield lower near-bottom dissipation and turbulent diffusivity values than our measurements, in spite of stronger near-bottom currents [*Bouffard et al*., 2012]; while the lateral extent of Lake Erie's central basin is comparable to Lake Michigan, it is a shallow basin for which the bottom boundary layer is strongly impacted by the overlying stratification.

Finally, it is important to begin to interpret our measurements in the context of the original motivation for the study, the ability of invasive quagga mussels to filter the deeper waters of Lake Michigan. Our measurements were obtained from a field site where the density of invasive bivalves is high. However, our fitted drag coefficient and roughness values (and those of *Valipour et al*. [2015a] from Lake Erie, which also has high quagga mussel densities) are very consistent with those (albeit very limited, i.e., derived from 5 velocity profiles) high-speed values obtained by *Saylor and Miller* [1988] in Lake Michigan, prior to infestation by either zebra or quagga mussels. Our values are higher than what was indirectly estimated by *Ivey and Boyce* [1982] in Lake Erie (prior to zebra or quagga mussel arrival; $C_{d1m} = 0.0033$) using a bulk approach. Putting more credence in the values derived from direct measurements of the logarithmic layer, these results suggest that the invasive mussels do not have a strong influence on the overlying flow (in spite of the ecosystem havoc they have wreaked [e.g., *Vanderploeg et al*., 2010]). The exceptions may be very weak flow conditions ($u_{1m} < 1$ cm s^{-1}), for which elevated drag and roughness values were found. Actively pumping bivalves are expected have a larger relative influence on the overlying flow during periods of weak flow; studies in laboratory flumes have pointed out the potential importance of mussel pumping in weak flow conditions, suggesting that mussel filtration causes a near-bed internal boundary layer that may alter turbulence and mean flow characteristics [*van Duren et al*., 2006; *Crimaldi et al*., 2007]. However, our study did not resolve the flow within the bottom 0.19 m of the water column, so what we may be resolving is the effect of active mussel filtration on the overlying flow. This is a hypothesis in need of future examination.

Simple law-of-the-wall estimates of the turbulent diffusion coefficient (Figures 12 and 15; Table 2), coupled with estimates of the turbulent boundary layer thickness, suggest an average turbulent mixing timescale of O (hours) ($\approx H^2 K_z^{-1}$, where H is the turbulent boundary layer thickness and K_z is the vertical turbulent mixing coefficient). In contrast, the observed mussel densities and laboratory-derived pumping rates suggest effective clearance rates of $\alpha \sim 20$ m/d, with corresponding boundary layer filtration timescales of $H/\alpha \sim$ O (hours), following arguments by *Koseff et al.* [1993]. With comparable mixing and filtration timescales, this suggests that mussel filtration will not be limited by mixing within the bottom boundary layer, in which case it will likely be limited by delivery from the quiescent hypolimnetic waters above the bottom boundary layer. Future studies should aim to characterize the turbulence – and weak stratification - in the entire turbulent bottom boundary layer, in order to more directly address these hypotheses.

Acknowledgments

This work was supported by Illinois-Indiana Sea Grant College Program (project # NAOAR4170095) and NSF grant OCE-1030842 (Physical Oceanography Program) to Purdue University. The authors thank Dennis Lyn and Matthew Brennan for helpful manuscript comments, Jun Choi for help with instrumentation and data analysis, graduate students at the University of Wisconsin-Milwaukee Water Institute for help with episodic sampling, and the captain, crew and scientists of the EPA R/V Lake Guardian for help with the mooring deployment and retrieval. Velocity and temperature data can be made available upon request, by emailing C. Troy at troy@purdue.edu.

References

Ackerman, J. D., M. R. Loewen, and P. F. Hamblin (2001), Benthic-pelagic coupling over a zebra mussel reef in western Lake Erie, *Limnol. Oceanogr.*, *46(4)*, 892–904.

Ahmed, S., C. D. Troy, and N. Hawley (2014), Spatial structure of internal Poincaré waves in Lake Michigan, *Environ. Fluid Mech.*, *14(5)*, 1229–1249.

Anderson, E. J., and D. J. Schwab (2013), Predicting the oscillating bi-directional exchange flow in the Straits of Mackinac, *J. Great Lakes Res.*, *39*(4), 663–671.

ASTM D422-63 (1998), *Standard test method for particle-size analysis of soils*, ASTM International, West Conshohocken, PA.

Bai, X., J. Wang, D. J. Schwab, Y. Yang, L. Luo, G. A. Leshkevich, and S. Liu (2013), Modeling 1993-2008 climatology of seasonal general circulation and thermal structure in the Great Lakes using FVCOM, *Ocean Modell.*, *65*, 40–63.

Beletsky, D., and D. J. Schwab (2001), Modeling circulation and thermal structure in Lake Michigan: Annual cycle and interannual variability, *J. Geophys. Res.*, *106*(C9), 19,745–19,771, doi:10.1029/2000JC000691.

Beletsky, D., D. J. Schwab, P. J. Roebber, M. J. McCormick, G. S. Miller, and J. H. Saylor (2003), Modeling wind-driven circulation during the March 1998 sediment resuspension event in Lake Michigan, *J. Geophys. Res.*, *108*(C2), *3038*, doi:10.1029/2001JC001159.

Boegman, L., M. R. Loewen, P. F. Hamblin, and D. A. Culver (2008), Vertical mixing and weak stratification over zebra mussel colonies in western Lake Erie, *Limnol. Oceanogr. Methods*, *53*(3), 1093.

Bouffard, D., L. Boegman, and Y. R. Rao (2012), Poincaré wave-induced mixing in a large lake, *Limnol. Oceanogr. Methods*, *57*(4), 1201–1216.

Bowden, K. F. (1978), Physical problems of the benthic boundary layer, *Geophys. Surv.*, *3(3)*, 255–296.

Caldwell, D. R., and T. M. Chriss (1979), The viscous sublayer at the sea floor, *Science*, *205(*4411*)*, 1131–1132.

Choi, J., C. D. Troy, T. C. Hsieh, N. Hawley, and M. J. McCormick (2012), A year of internal Poincaré waves in southern Lake Michigan, *J. Geophys. Res.*, *117*, C07014, doi:10.1029/2012JC007984.

Choi, J. M., C. D. Troy, and N. Hawley (2015), Shear dispersion from near-inertial internal Poincaré waves in large lakes, *Limnol. Oceanogr. Methods*, *60*(6), 2222–2235, doi:10.1002/lno.10163.
Churchill, J. H., A. J. Williams, and E. A. Ralph (2004), Bottom stress generation and sediment transport over the shelf and slope off of Lake Superior's Keweenaw peninsula, *J. Geophys. Res.*, *109*, C10S04, doi:10.1029/2003JC001997.
Cossu, R., and M. G. Wells (2013), The interaction of large amplitude internal seiches with a shallow sloping lakebed: Observations of benthic turbulence in Lake Simcoe, Ontario, Canada, *PLoS ONE*, *8*(3), e57444.
Crimaldi, J. P., J. R. Koseff, and S. G. Monismith (2007), Structure of mass and momentum fields over a model aggregation of benthic filter feeders, *Biogeosciences*, *4*(1), 269–282.
Cushman-Roisin, B., and J. M. Beckers (2011), *Introduction to Geophysical Fluid Dynamics: Physical and Numerical Aspects*, Academic Press, Oxford, UK.
Friedrichs, C. T., and L. D. Wright (1997), Sensitivity of bottom stress and bottom roughness estimates to density stratification, Eckernförde Bay, southern Baltic Sea, *J. Geophys. Res.*, *102*(C3), 5721–5732, doi:10.1029/96JC03550.
Grant, W. D., and O. S. Madsen (1986), The continental-shelf bottom boundary layer, *Annu. Rev. Fluid Mech.*, *18*(1), 265–305.
Grant, W. D., A. J. Williams III, and S. M. Glenn (1984), Bottom stress estimates and their prediction on the northern California continental shelf during CODE-1: The importance of wave-current interaction, *J. Phys. Oceanogr.*, *14*(3), 506–527.
Hawley, N., and B. M. Lesht (1995), Does local resuspension maintain the benthic nepheloid layer in southeastern Lake Michigan?, *J. Sediment. Res., Sect. A*, *65*(1), 69–76.
Ivey, G. N., and F. M. Boyce (1982), Entrainment by bottom currents in Lake Erie, *Limnol. Oceanogr.*, *27*(6), 1029–1038.
Koseff, J. R., J. K. Holen, S. G. Monismith, and J. E. Cloern (1993), Coupled effects of vertical mixing and benthic grazing on phytoplankton populations in shallow, turbid estuaries, *J. Mar. Res.*, *51*(4), 843–868.
Lee, C., D. J. Schwab, D. Beletsky, J. Stroud, and B. Lesht (2007), Numerical modeling of mixed sediment resuspension, transport, and deposition during the March 1998 episodic events in southern Lake Michigan, *J. Geophys. Res.*, *112*, C02018, doi:10.1029/2005JC003419.
Ligrani, P. M., and R. J. Moffat (1986), Structure of transitionally rough and fully rough turbulent boundary layers, *J. Fluid Mech.*, *162*, 69–98.
Lorke, A. (2007), Boundary mixing in the thermocline of a large lake, *J. Geophys. Res.*, *112*, C09019, doi:10.1029/2006JC004008.
Lorke, A., L. Umlauf, T. Jonas, and A. Wüest (2002), Dynamics of turbulence in low-speed oscillating bottom-boundary layers of stratified basins, *Environ. Fluid Mech.*, *2*(4), 291–313.
Lueck, R. G., and L. Lu (1997), The logarithmic layer in a tidal channel, *Cont. Shelf Res.*, *17*(14), 1785–1801.
Luo, L., J. Wang, D. J. Schwab, H. Vanderploeg, G. Leshkevich, X. Bai, H. Hu, and D. Wang (2012), Simulating the 1998 spring bloom in Lake Michigan using a coupled physical-biological model, *J. Geophys. Res.*, *117*, C10011, doi:10.1029/2012JC008216.
Mellor, G. (2002), Oscillatory bottom boundary layers, *J. Phys. Oceanogr.*, *32*, 3075–3088.
Monismith, S. G., J. R. Koseff, J. K. Thompson, C. A. O'Riordan, and H. M. Nepf (1990), A study of model bivalve siphonal currents, *Limnol. Oceanogr.*, *35*(3), 680–696.
Mosley, C., and H. Bootsma (2015), Phosphorus recycling by profunda quagga mussels (Dreissena rostriformis bugensis) in Lake Michigan, *J. Great Lakes Res.*, 38–48, doi:10.1016/j.jglr.2015.07.007.
Nielsen, P. (2005), *Coastal Bottom Boundary Layers and Sediment Transport*, World Sci., Singapore.
Peine, F., B. Bobertz, B., and G. Graf (2005), Influence of the blue mussel Mytilus edulis (Linnaeus) on the bottom roughness length (z0) in the south-western Baltic Sea, *Baltica*, *18*(1), 13–22.
Perlin, A., J. N. Moum, J. M. Klymak, M. D. Levine, T. Boyd, and P. M. Kosro (2005), A modified law-of-the-wall applied to oceanic bottom boundary layers, *J. Geophys. Res.*, *110*, C10S10, doi:10.1029/2004JC002310.
Perlin, A., J. N. Moum, J. M. Klymak, M. D. Levine, T. Boyd, and P. M. Kosro (2007), Organization of stratification, turbulence, and veering in bottom Ekman layers, *J. Geophys. Res.*, *112*, C05S90, doi:10.1029/2004JC002641.
Plattner, S., D. M. Mason, G. A. Leshkevich, D. J. Schwab, and E. S. Rutherford (2006), Classifying and forecasting coastal upwellings in Lake Michigan using satellite derived temperature images and buoy data, *J. Great Lakes Res.*, *32*(1), 63–76.
Pollard, R. T., P. B. Rhines, and R. O. Thompson (1972), The deepening of the wind-mixed layer, *Geophys. Fluid Dyn.*, *4*(1), 381–404.
Pope, S. B. (2000), *Turbulent Flows*, Cambridge Univ. Press, Cambridge, U. K.
Ravens, T. M., O. Kocsis, and A. Wüest (2000), Small-scale turbulence and vertical mixing in Lake Baikal, *Limnol. Oceanogr.*, *45*(1), 159–173.
Saylor, J. H., and G. S. Miller (1988), Observation of Ekman veering at the bottom of Lake Michigan, *J. Great Lakes Res.*, *14*(1), 94–100.
Sternberg, R. W. (1968), Friction factors in tidal channels with differing bed roughness, *Mar. Geol.*, *6*, 243–260.
Sternberg, R. W. (1970), Field measurements of the hydrodynamic roughness of the deep-sea boundary, *Deep Sea Res. Oceanogr. Abstr.*, *17*(3), 413–420.
Taylor, J. R., and S. Sarkar (2008), Stratification effects in a bottom Ekman layer, *J. Phys. Oceanogr.*, *38*(11), 2535–2555.
Tennekes, H. (1973), The logarithmic wind profile, *J. Atmos. Sci.*, *30*(2), 234–238.
Troy, C. D., S. Ahmed, N. Hawley, and A. Goodwell (2012), Cross-shelf thermal variability in southern Lake Michigan during the stratified periods, *J. Geophys. Res.*, *117*, C02028, doi:10.1029/2011JC007148.
Valipour, R., D. Bouffard, and L. Boegman (2015a), Parameterization of bottom mixed layer and logarithmic layer heights in central Lake Erie, *J. Great Lakes Res.*, *41*, 707–718.
Valipour, R., D. Bouffard, L. Boegman, and Y. R. Rao (2015b), Near-inertial waves in Lake Erie, *Limnol. Oceanogr. Methods*, *60*(5), 1522–1535.
Van der Lee, E. M., and L. Umlauf (2011), Internal wave mixing in the Baltic Sea: Near-inertial waves in the absence of tides, *J. Geophys. Res.*, *116*, C10016, doi:10.1029/2011JC007072.
Vanderploeg, H. A., J. R. Liebig, T. F. Nalepa, G. L. Fahnenstiel, and S. A. Pothoven (2010), *Dreissena* and the disappearance of the spring phytoplankton bloom in Lake Michigan, *J. Great Lakes Res.*, *36*, 50–59.
van Duren, L. A., P. M. J. Herman, A. J. J. Sandee, and C. H. R. Heip (2006), Effects of mussel filtering activity on boundary layer structure, *J. Sea Res.*, *55*(1), 3–14.
Van Rijn, L. C. (1993), *Principles of Sediment Transport in Rivers, Estuaries and Coastal Seas*, Aqua Publ., Amsterdam.

Weatherly, G. L., and P. J. Martin (1978), On the structure and dynamics of the oceanic bottom boundary layer, *J. Phys. Oceanogr.*, *8*(4), 557–570.

Wengrove, M. E., and D. L. Foster (2014), Field evidence of the viscous sublayer in a tidally forced developing boundary layer, *Geophys. Res. Lett.*, *41*, 5084–5090, doi:10.1002/2014GL060709.

Wimbush, M., and W. Munk (1970), The Benthic boundary layer, in *The Sea*, vol. 4, Part I, edited by A. E. Maxwell, pp. 730–758, Wiley-Interscience, N. Y.

Zilitinkevich, S., A. Baklanov, J. Rost, A. S. Smedman, V. Lykosov, and P. Calanca (2002), Diagnostic and prognostic equations for the depth of the stably stratified Ekman boundary layer, *Q. J. R. Meteorol. Soc.*, *128*(579), 25–46.